Numerical simulation of subcooled and superheated jets under thermodynamic non-equilibrium

Konstantinos Lyras[1], Jennifer Wen[2], Siaka Dembele[1], D.P. Schmidt[3]
[1]Kingston University London, Department of Mechanical and Automotive Engineering, London, UK.
Email: jennifer.wen@warwick.ac.uk
[2]University of Warwick, School of Engineering, Coventry, UK
[3]University of Massachusetts Amherst, MIE Department, MA 01003, USA

Abstract

Modelling and simulating the rapid pressure drop inside nozzles is a significant challenge because of the complexity of the multiple associated phenomena. In the present study, FlashFOAM a compressible solver for calculating the phase change within various nozzle geometries undergoing rapid pressure drops has been developed in the frame of the open source Computational Fluid Dynamics (CFD) code OpenFOAM. FlashFOAM accounts for the inter-phase heat transfer with the Homogeneous Relaxation Model (HRM). The work describes the development of a pressure equation within a different formulation than in other studies. The surface forces due to liquid-gas interfacial instabilities are modelled here in a novel coupling of HRM with the volume of fluid method giving rise to a conservative method for modelling primary atomisation. This new pressure equation is validated with published experimental measurements. A validation series dedicated to long nozzles is included for the first time. Novel additional tests for the flow characteristics and vapour generation in cryogenic liquid cases are included showing that the solver can be employed to gain some new insights into the physics of the flow regimes of sudden depressurising cryogenic liquids. The dependency of the geometry of the nozzles, pressure and subcooled degree on the vapour generation has been analysed including the effect of turbulence on the nozzle flow avoiding the laminar flow scenarios of previous validation studies. The validation study has demonstrated that FlashFOAM can be used to simulate flash boiling scenarios accurately and predict the properties of flash atomisation.

Keywords: Flash boiling, two-phase flows, thermal non-equilibrium.

1. Introduction

Flashing is a complex process involving multiphase flows that usually occurs during the sudden depressurisation of a fluid stored under high pressure and high temperatures. Typical industrial scenarios involve accidental releases through cracks in pipes and vessels. Other applications include fuel spray atomisation during injection in internal combustion (IC) engines and loss of coolant accidents in nuclear power plants. In all these cases the release results in a spray at the nozzle exit which disperses following turbulent mixing, aerodynamic breakup and droplet collisions. The whole process of flashing is not entirely understood experimentally, but in general, its stages are divided into nucleation, bubble growth, and atomisation (Oza, 1983). Flashing can occur either inside or outside the nozzle depending on the local pressure and geometry among others, and the vapour generation leads to interfacial interactions that eventually influence the spray properties.

A key aspect of flashing is bubble nucleation. The flashing phenomenon may happen in the case of a superheated or a subcooled liquid following either an isothermal or an isobaric process which corresponds to a metastable state where liquid and vapour co-exist. Flashing inception starts when, inside the saturation dome, the liquid exists in a metastable state.

Bubble formation and growth in two-phase mixtures within nozzles have a significant impact on the atomisation and the spray dynamics. Depending on the vaporisation rate and conditions the flow pattern might be bubbly, slug or annular. Sher (2008) and Park and Lee (1994) provided a detailed regime analysis. They also successfully predicted the mass flow rate and the resulting jet dispersion. Different modelling strategies have been developed for simulating flashing flows inside pipes. If the bubble distribution is such that there is no or very little relative velocity (slip velocity) between the two phases, then the flow can be considered homogeneous and if the slip velocity cannot be ignored the flow is separated. Homogeneous Equilibrium Model (HEM) is the most common critical flow model which assumes zero slip velocity. It assumes that mass, momentum and energy transfer

between the phases happens rapidly enough so that equilibrium is reached. The HEM model seems to work very well in non-isentropic liquid expansion cases and long pipes where the flow has sufficient time to reach equilibrium (Salvador et al. 2017). However, the predicted mass flow rates can be very large compared to experiments, and in cases of short nozzles where there is not sufficient time for vapour generation to reach equilibrium, the difference between the prediction and the exact value can be 25% according to Schroder and Nha (1987). An improvement was proposed by Fauske (1962) taking into account the slip velocity S, estimating that the maximum mass flow rate is achieved at $S^{1/2}$ using momentum balance at the nozzle exit. Along the same direction, Moody (1965), using an energy balance, proposed that the maxima to mass flow rate occur at $S^{1/3}$. Deviations with the actual experimental critical mass flow rates exist using these models, with the calculated values being usually higher than in HEM, and the unphysical values of S are a significant constraint. In the models of Fauske and Moody, mass flow rate estimation is treated in the same way for short and long nozzles e.g. by extracting from a formulation that includes only the thermophysical properties of the fluid which are usually stagnation pressure and degree of superheat (or subcooling). Zaloudek (1964) and Xu (1999) among others showed that the geometry could play an important role in the case of depressurisation inside pipes. In such cases, the above mentioned models fail to predict the experimental mass flow rates resulting in underepredictions, which can be attributed to the underlying assumption of thermodynamic equilibrium, which is a convenient approach that leads to a set of equations that under certain circumstances can be solved for the multiphase flow across the nozzle. For example, in HEM one might obtain a one-fluid formulation suitable for small-scale cavitating flows. The latter is commonly used in some open source CFD codes (Karrholm et al. 2007).

One of the most widely known and among the oldest models for thermal non-equilibrium in two-phase critical discharges was proposed by Henry et al. (1970) who considered the flow as frozen and hence no phase change occurs, a concept that could be valid for small flow timescales like within short nozzles. The non-equilibrium is handled with a coefficient which is a function of the fraction of the equilibrium vapour. Downar-Zapolski et al. (1996) proposed the Homogeneous Relaxation Model (HRM) which accounts for the non-equilibrium vapour generation. The model estimates the rate of change of the local vapour quality. The concept of the relaxation term which has its origin back to Einstein's (1920) work for sound propagation in dissociated gases and others, expresses a physical reality, i.e. the instant vapour mass fraction would relax to the equilibrium value over a proposed timescale. The values of the timescale are linked to the interphase mass transfer in a way that will be described in the next section. The model might have a behaviour similar to the frozen flow model or the HEM depending on whether the timescale for relaxation is high or low. Although older modelling approaches were based on an 1-D thinking, when moving to multidimensional modelling, the HEM and HRM are really only homogeneous on the sub-grid scale level, which is less restrictive than 1-D.

There are two families of numerical methods to simulate dispersed flows with various advantages and disadvantages. In the two-fluid approach, each phase has its velocity, and the continuity equation is solved for the liquid and vapour phase whereas in the one-fluid approach the flow characteristics are averaged between the two phases offering a simpler formulation. Maksic et al. (2002) used a four-equation model to simulate flashing in converging-diverging geometries employing a scalar transport equation for the bubble number density (number of bubbles per unit volume) assuming that the vapour always stayed in the saturation condition overpredicting the void fraction. Other two-fluid models choose to drop the initial bubble formation presuming a size and distribution of the bubbles which can be attributed as a major constraint. However, the bubble nucleation can be random across the flow direction, and there is unsufficient evidence to support such a simplification, at least for the majority of flash boiling flows (Rusche, 2002).

Regarding the one-fluid approaches, Bianchi (2008) developed a one-dimensional model for flash evaporation. A one-dimensional mixture model formulation was employed to predict the influence of the superheat degree and geometry in flashing and atomisation. He took into account the thermal non-equilibrium via the HRM. The relaxation timescale was calculated by considering the temperature change in the vapour phase. The model showed that when increasing the superheat degree, the bubble nucleation was enhanced with atomisation following possibly the same mechanism described by Fujimoto (1994). The impact of the nozzle geometry, regarding the boiling process will be discussed in the results section.

An attempt to exploit the efficiency of the HRM in two-dimension simulations was made by Lee et al. (2009). They used a fully Eulerian approach using the Pressure-Implicit-Split-Operator (PISO) algorithm. Given the fact that the pressure evaluation is associated to phase change a relaxation term is included in the PISO algorithm. The model was validated for superheated water flowing within nozzles with relatively small length-to-diameter ratios (abbreviated as L/D hereafter) and constant pressure cases. Results showed that combining HRM with one-fluid compressible two-phase solvers, high fidelity simulations can be performed. Additional work has been conducted by Schmidt et al. (2010) who included one more term to account for the compressibility effects. Simulations were performed for flashing water initially superheated for L/D = 4. These were among the previous approaches to use HRM in CFD codes for simulating non-equilibrium flows inside pipes and nozzles. Wen et al. (2013, 2016) used the same model to model carbon-dioxide releases using a relaxation time of 0.1 ms.

In the present study, numerical investigations have been carried out to gain insight of the phenomena triggered by the rapid pressure drop inside the nozzle and evaluate how the jet regime changes with respect to geometry and initial thermodynamic state. The development of FlashFOAM , within the frame of open source CFD code, OpenFOAM, to simulate two-phase flows under sudden depressurization will firstly be described. It simulates the rapid evaporation in the presence of the pressure waves travelling across the domain using a compressible approach that couples the Navier-Stokes equations with the HRM. FlashFOAM follows the same approach of Schmidt et al. (2010) to construct a pressure equation that takes into consideration the interphase heat and mass transfer. The method is based on the volume of fluid approach, and turbulence modelling which is absent in previous works of Lee et al. (2009) and Schmidt at al. (2010), and the performance of the Jones-

Launder $k-\varepsilon$ model is tested in an attempt to develop a unified treatment from the internal flow boiling to the atomisation and the emerging spray. The presence of ambient air is included in the calculations, so that its influence on the critical mass flow rates is considered. FlashFOAM has been validated for the predictions of flashing flows through both long nozzles where traditionally HEM performs well, as well as short nozzles where the insufficient time for the vapour to equilibriate makes HEM less reliable. Important flow characteristics such as the void fraction and velocity along the nozzle are obtained giving an insight of the jet regime in different stages. The impact on the metastable jet of the stagnation pressure and the subcooling degree is studied together with a qualitative analysis on the behaviour of cryojenic jets under flashing through sharp-edged nozzles.

2. Mathematical and Numerical Formulations

2.1 *Mass, momentum and energy equations*

The following equations of mass and momentum are solved in a fully Eulerian framework. The liquid and vapour phases are considered to have the same velocity. The enthalpy equation is dropped in isenthalpic simulations. The compressible formulations used follow that of Prosperetti et al. (2006):

$$\frac{\partial \rho}{\partial t}+\frac{\partial \rho u_j}{\partial x_j}=0 \tag{1}$$

$$\frac{\partial \rho u_i}{\partial t}+\frac{\partial \rho u_i u_j}{\partial x_j}=-\frac{\partial \mathrm{p}}{\partial \mathrm{x}_i}+\frac{\partial \tau_{ij}}{\partial x_j}+F_\sigma \tag{2}$$

$$\frac{\partial \rho h}{\partial t}+\frac{\partial \rho u_j h}{\partial \mathrm{x}_j}=\frac{Dp}{Dt}+\frac{\partial}{\partial \mathrm{x}_j}\left(\alpha_{eff}\frac{\partial \mathrm{h}}{\partial \mathrm{x}_j}\right)+\tau_{ij}\frac{\partial u_i}{\partial \mathrm{x}_j} \tag{3}$$

$$\frac{\partial \rho \gamma}{\partial t}+\frac{\partial \rho u_i \gamma}{\partial x_i}=\frac{\partial}{\partial x_i}\left(\frac{\mu_t}{Sc_t}\frac{\partial \gamma}{\partial \mathrm{x}_i}\right) \tag{4}$$

where ρ, p, h, μ_t, Sc_t are the mixture density, pressure, enthlpy, turbulent kinematic viscosity and turbulent Schmidt number with $Sc_t=\mu_t/\rho D_m$, and D_m denoting the mass diffusivity. Here, the velocity at x_j direction is indicated with u_j. In Newtonian fluids the deviatoric viscous stress tensor, is calculated with the viscosity μ and the strain rate tensor $S_{ij,}$ where $S_{ij}=1/2(\partial u_i/\partial x_j+\partial u_j/\partial x_i)$, as $\tau_{ij}=2\mu S_{ij}-\frac{2}{3}\mu\delta_{ij}S_{kk}$, where δ_{ij} is the Kronecker symbol). The source term due to surface tension, is denoted with F_σ, and will be discussed latter. The enthalpy equation contains the material derivative of pressure ($Dp/D\,t$) and the shear heating source term. Here γ is the fuel mass fraction (liquid and vapour) with a simple diffusion term on the right hand side. The advantage on this approach is that it accounts for the presence of air inside the nozzle and the explicit calculation of the liquid mass fraction via an appropriate phase change model described in the next section. The mixture density ρ is in case of pure liquid-vapour mixture the mean value of the liquid and vapour and α_{eff} is the effective thermal diffusivity of the mixture.

2.2 *Thermal Non-Equilibrium Phase Change*

The vapour mass fraction x is given by the following transport equation:

$$\frac{\partial \rho x}{\partial t}+\frac{\partial \rho u_i x}{\partial x_i}=\Gamma \tag{5}$$

The last term in Eq. (5) is the vapour generation rate and must be modelled as will be explained in the next section. This term plays a fundamental role in the flashing process, reflecting the whole complicated phenomenon of flashing and depends not only on the flow parameters but also on the structure of pre-existing interfaces of the metastable liquid. The Eqs. (1) – (5) form a set of equations that needs additional closures to solve. One possible modelling approach for the quality equation is to consider a diffusivity/turbulent flux diffusion model employing a Fick-like expression as follows,

$$\frac{\partial \rho x}{\partial t} + \frac{\partial \rho u_j x}{\partial x_j} = \Gamma = \frac{\partial}{\partial x_j}\left(\frac{\mu_t}{Sc_t}\frac{\partial \mathrm{x}}{\partial x_j}\right) - x\frac{p_v - p_{sat}}{\Theta p_{sat}} \tag{6}$$

Here p_v, p_{sat} are the vapour and saturation pressure, and Θ a relaxation time corresponding to the time needed for relaxation to equilibrium. The model was previously used by Wen et al. (2013, 2016) and Wareing (2014) for non-equilibrium releases but both group of authors used a constant relaxation timescale for the whole flow. For this reason, the HRM of Downar-Zapolski et al. (1996) , which assumes that the instantaneous vapour mass fraction x relaxes at the local equilibrium value, $\bar{x}$ through a timescale Θ, is used as the basis of the present syudy. The first order approximation of the term Γ is given as follows,

$$\Gamma = \rho\frac{Dx}{Dt} = \rho\frac{\bar{x} - x}{\Theta} \tag{7}$$

The equilibrium quality $\bar{x}$ can be calculated either assuming isentropic or isenthalpic conditions. Experiments from Reinke and Yadigaroglu (2001) for superheated liquids under sudden high depressurization indicated that the vapor qualities obtained, were close to the isenthalpic line so the isenthalpic formulation is used here,

$$\bar{x} = \frac{h - h_{l,sat}}{h_{v,sat} - h_{l,sat}} \tag{8}$$

Here, the liquid and vapour enthalpies denoted as $h_{l,sat}$, $h_{v,sat}$ are calculated at the saturation conditions. Knowing the void fraction $\alpha = (\rho_l - \rho)/(\rho_l - \rho_v)$, the quality can be directly computed as,

$$x = \alpha\frac{\rho_v}{\rho} \tag{9}$$

The timescale Θ then calculated considering the local flow characteristics using the following relationship,

$$\Theta = \Theta_0 \alpha^{-0.54}\psi^{-1.76} \tag{10}$$

Where Θ_0 is a constant with time dimensions and is equal to $3.84 \cdot 10^{-7}$, and ψ dimensionless pressure given by,

$$\psi = \left|\frac{p_{sat} - p}{p_{crit} - p_{sat}}\right| \tag{11}$$

Equations (9)-(10) have been derived from Downar-Zapolski et al. for flashing water and are valid for pressures higher than 10 bar.

2.3 *Pressure equation*

The derivation of pressure equation developed by Schmidt (2010) will be discussed here. The concept of the model arises from the work of Bilicki and Kerstin (1990). The density is a function of pressure, quality and enthalpy, that is to say, $\rho = \rho(p, h, x)$. So the derivative of the density is,

$$\frac{D\rho}{Dt} = D_1 \frac{Dp}{Dt} + D_2 \frac{Dh}{Dt} + D_3 \frac{Dx}{Dt} \tag{12}$$

$$D_1 = \left.\frac{\partial \rho}{\partial p}\right|_{h,x}, D_2 = \left.\frac{\partial \rho}{\partial h}\right|_{p,x}, D_3 = \left.\frac{\partial \rho}{\partial x}\right|_{p,h} \tag{13}$$

Here the D/Dt operator is the material derivative. Considering the boiling process as isenthalpic, the second term in Eq. (13) drops out. Combining it with the mass equation, the following can be obtained:

$$-\rho \frac{\partial u_i}{\partial x_i} = \left.\frac{\partial \rho}{\partial p}\right|_{x,h} \frac{Dp}{Dt} + \left.\frac{\partial \rho}{\partial x}\right|_{p,h} \frac{Dx}{Dt} \tag{14}$$

Some of the terms in the momentum equation are linear, and some are quadratic with respect to velocity. Hence, linearizing all the terms, Eq. (2) can be writen with matrix notation (see Jasak (1996)),

$$a_P u_P = H(u_j) - \frac{\partial \mathrm{p}}{\partial x_i} + F_\sigma \tag{15}$$

In this semi-discretised form of momentum equation, the diagonal coefficients tensor $a_P$is a function of velocity. The $H(u_j)$ term consists of the matrix coefficients for all neighbours multiplied by corresponding velocities and the source parts of the transient terms and all other source terms (except for the pressure gradient). Solving Eq. (15) for u_P and substituting it into Eq. (14) together with directly inserting Eq. (7), a formula for pressure is obtained without the pressure gradient correction. Including the effect of mixture/air in the pressure equation, the following term should be added,

$$\left.\frac{\partial \rho}{\partial \gamma}\right|_{p,h} \frac{D\gamma}{Dt} \tag{16}$$

The matrix equation finally becomes:

$$\rho \frac{\partial}{\partial x_j}\left(\frac{1}{a_p} H(u_j)\right)_f - \rho \frac{\partial}{\partial x_j}\left(\frac{1}{\alpha_p}\frac{\partial \mathrm{p}}{\partial x_i}\right) + \rho \frac{\partial}{\partial x_j}\left(\frac{1}{a_p} F_\sigma\right) + \left.\frac{\partial \rho}{\partial p}\right|_{x,h} \frac{Dp}{Dt} + \left.\frac{\partial \rho}{\partial x}\right|_{p,h} \frac{\bar{x}-x}{\Theta} + \left.\frac{\partial \rho}{\partial \gamma}\right|_{p,h} \frac{D\gamma}{Dt} = 0 \tag{17}$$

The operator $()_f$ implies interpolation in the cell faces. The term $\partial\rho/\partial p$ is the isenthalpic compressibility of the mixture and is the weighted average of the liquid and vapour compressibilities, $\Psi_l = 1/a_l^2, \Psi_v = 1/a_v^2$ respectively, where α_l, α_v are the liquid and vapour speed of sound. The density is calculated from,

$$\rho = \gamma((1-x)\rho_l + x\rho_v) + (1-\gamma)\rho_{air} \tag{18}$$

The liquid and vapour densities in the mixture are related to pressure via the following equations,

$$\rho_l = \rho_{l,ref} + \Psi_l(p - p_{sat}) \tag{19}$$

$$\rho_v = \rho_{v,ref} + \Psi_l(p - p_{sat}) \quad (20)$$

where a reference state is used, $\rho_{l,ref}, \rho_{v,ref}$ for the densities.

2.4 *Turbulence modelling*

Turbulence is modelled using the Reynolds-averaged Navier–Stokes (RANS) approach. Each variable Φ is split into an averaged $\bar{\Phi}$ and a fluctuating part $\acute{\Phi}$. The mass weighted Favre averaged $\tilde{\Phi} = \overline{\rho\Phi}/\bar{\Phi}$. Equations (1)-(3) can be written as,

$$\frac{\partial \bar{\rho}}{\partial t} + \frac{\partial \bar{\rho}\tilde{u}_i}{\partial x_i} = 0 \quad (21)$$

$$\frac{\partial \bar{\rho}\tilde{u}_i}{\partial t} + \frac{\partial \bar{\rho}\tilde{u}_j\tilde{u}_i}{\partial x_j} = -\frac{\partial \bar{p}}{\partial x_i} + \frac{\partial \bar{\rho}\tilde{R}_{ij}}{\partial x_j} \quad \text{, where } R_{ij} = u_i'u_j' \quad (22)$$

$$\frac{\partial \bar{\rho}\tilde{h}}{\partial t} + \frac{\partial \bar{\rho}\tilde{u}_j\tilde{h}}{\partial x_j} = \frac{D\bar{p}}{Dt} + \frac{\partial}{\partial x_j}\left(\alpha_{eff}\frac{\partial \tilde{h}}{\partial x_j}\right) + \overline{\tau_{ij}\frac{\partial u_i}{\partial x_j}} \quad (23)$$

Additionally, the equation of the whole mixture $\tilde{\gamma}$ of liquid and vapour is solved in order to include air entaintment effects. This is,

$$\frac{\partial \bar{\rho}\tilde{\gamma}}{\partial t} + \frac{\partial \bar{\rho}\tilde{u}_j\tilde{\gamma}}{\partial x_j} = \frac{\partial}{\partial x_j}\left(\frac{\mu_t}{Sc_t}\frac{\partial \tilde{\gamma}}{\partial x_j}\right) \quad (24)$$

The eddy or turbulent viscosity is defined as $\mu_t = \rho C_\mu k^2/\varepsilon$. The turbulent kinetic energy k and the turbulence energy dissipation ε are then calculated as,

$$\frac{\partial \rho k}{\partial t} + \frac{\partial \rho u_i k}{\partial x_i} = \frac{\partial}{\partial x_j}\left[(\mu + \mu_t)\frac{\partial k}{\partial x_j}\right] - \bar{\rho}\widetilde{\acute{u}_i\acute{u}_j}\frac{\partial u_j}{\partial x_i} - \rho\varepsilon \quad (25)$$

$$\frac{\partial \rho \varepsilon}{\partial t} + \frac{\partial \rho u_i \varepsilon}{\partial x_i} = \frac{\partial}{\partial x_j}\left[(\mu + \mu_t)\frac{\partial \varepsilon}{\partial x_j}\right] - \bar{\rho}\widetilde{\acute{u}_i\acute{u}_j}\frac{\partial \tilde{u}_j}{\partial x_i} - C_{1\varepsilon}\frac{\varepsilon}{k}(\bar{\rho}\widetilde{\acute{u}_i\acute{u}_j}\frac{\partial \tilde{u}_j}{\partial x_i} - C_{2\varepsilon}\bar{\rho}\frac{\varepsilon^2}{k} \quad (26)$$

The constant $C_{1\varepsilon} = 1.6$, $C_{2\varepsilon} = 1.92$, $C_\mu = 0.09$ and the classical Boussinesq eddy viscosity assumption are used. The SST $k - \omega$ model of Menter (1993) , which is expected to perform well in the near wall regions and used successfully by Liao (2015) for flashing inside long converging-diverging nozzle, has also been tested.

2.5 Volume-of-Fluid method

In cases of sudden depressurisation through pipes, cavities are generated at the sharp inlet corners extending up to the nozzle exit. The surface forces due to the liquid-gas intefacial instabilites are modelled here. A VOF method to capture the interface between the liquid and gas phases is implemented. Resolving the surface forces is important in many situations including cases of cavitating cryogenic liquid (Ishimoto et al. 2009). VOF methods can resolve the inter-phase dynamics offering an explicit update for the evolution of liquid-gas mixture inside the nozzle. The method can aid the understanding of the cavitating/flashing jets mechanism. Previous methods of coupling HEM with VOF are reported (Srinivasan et al. 2010). Here the HRM is coupled with VOF in a novel formulation. A slightly different VOF approach from the one that is already embeded in OpenFOAM , has been adopted in the present study. Instead of solving a transport equation for liquid volume fraction, φ, the liquid mass fraction is employed after solving the equation for the vapour quality (equations are solved in a segratated approach). The liquid volume fraction is then updated offering a

compressible VOF formulation (Jiang et al. 2010). In the present study, the following simple expression is used,

$$\varphi = \frac{\gamma(1-x)(\rho_l-(\rho_l-\rho_v)x)}{\rho_l} \tag{27}$$

The surface tension force needs to be explicity estimated but the location and shape of the surface between the liquid and gas phase is not explicitly known. The classic continuum surface force (CSF) of Brackbill et al. (1992) is used which represents the surface tension impact as a continuous volumetric force acting within the interface. The force is given by,

$$F_\sigma = \sigma\kappa\nabla\varphi \tag{28}$$

where with σ is denoted the surface tension of the liquid and κ corresponds to the curvature of the interface and is given by,

$$\kappa = -\nabla\cdot\left(\frac{\nabla\varphi}{|\nabla\varphi|}\right) \tag{29}$$

VOF is capable of revealing more insight in the spray region as well as upstream the nozzle exit allowing the modelling of the primary atomisation and secondary break-up in a volume conservative way.

2.6 Numerical implementation

The segregated approach has been used as a general framework for the present work. The equations are solved sequentially with the finite volume method. The described model has been developed within the framework of the open source CFD code OpenFOAM® (Weller et al. 1998). The solver can handle unstructured polyhedral meshes of arbitrary shape. All variables are stored in the centre of the control volumes. Splitting equations of conservation laws lagging inter-equation coupling terms is sufficient in many cases for subsonic and sonic flows. Here the cases the model tested are very likely to reach the choking conditions while transversing the pressure spectrum of the available experimental data.

Since source term coupling plays an important role in the solution, a predictor-corrector step is used. The combination of the SIMPLE (Semi-implicit method pressure-linked equations) and the PISO (Pressure-Implicit with Splitting of Operators) algorithm is used to evaluate pressure. First, the discretised density equation is solved together with the quality equation. The finite difference representation of the convective and diffusive momentum fluxes, in order to increase stability and accuracy, is split into the diagonal and non-diagonal part.

The discretised momentum equation is solved implicitly using the old pressure $p^*$and density,

$$a_P u_i^* = H(u_i\ ) \tag{30}$$

The solution of this equation yields to a predicted velocity u_i^*. Following Issa (1986) and employing the continuity equation, a pressure equation is constructed based on Eq. (17), which comprises the derivative of density with respect to the quality and the HRM term for the phase change as described in the previous section. Solving the Eq. (17) gives the new pressure p^{**}.The solution is relaxed using the standard procedure explained in Patankar (1980). An under-relaxation factor of 0.4 is used for the current simulations for pressure. The new fluxes F are obtained after the non-orthogonal corrections from the following,

$$F = \left[\left(\frac{H(u_i^*)}{a_P}\right)_f - \left(\frac{1}{a_P}\right)_f \left(\frac{\partial p^{**}}{\partial x_i}\right)_f + (\sigma\kappa)_f \left(\frac{\partial \varphi}{\partial x_i}\right)_f\right] \cdot S_f \tag{31}$$

where S_f is the face area vector. When the pressure equation is satisfied the above formulation is guaranteed to be conservative. The corrected velocity denoted with u_i^{**} is obtained explicitly from,

$$u_i^{**} = \frac{1}{a_P}\left[H(u_i^*) + \sigma\kappa \frac{\partial \varphi}{\partial x_i} - \frac{\partial p^*}{\partial x_i}\right] \tag{32}$$

The PISO iterations used for the present work were no more than ten. After the latest pressure correction, the new velocity field is used to update the fluxes with the pressure gradient and the tensors $H(u_i^*), a_P$ so CourantCFL numbers larger than one can be accommodated. In this case, typically up to five PIMPLE iterations were needed and the CFL values were up to 2.5. The fluxes were calculated by interpolating the old values of velocity at the cell faces using a TVD scheme. A second order accuracy scheme that uses the least squares distance calculation for all neighbour cells was used for the gradient terms. The material derivatives added to the model introduce asymmetry, so a preconditioned bi-conjugate gradient method was used for velocity. The pressure boundary conditions are supposed to be fixed values for the inlet and a method that does not reflect waves described by Poinsot (1992) was employed. Finally, fixed values for the inlet velocity and zero gradients for the exit velocity were imposed.

3. Results and Discussion

3.1 *Validation*

Different test cases for validation are investigated and presented in this section. Typical experimental apparatus for flash boiling experiments consists of a high-pressure storage vessel, a flow passage and a low-pressure plenum. The initial conditions are either superheated or subcooled. Inlet pressure is an important parameter since the local pressure decreases as the liquid approaches the nozzle exit. At some point, it drops below the local saturation pressure where flashing is initiated.

The experiments of Jinliang et al. (1995) are considered first. The experiments involved two-phase critical releases of pressurised water in sharp-edged tubes. The channel connecting the high and low-pressure domains has length $L = 4.0\,mm$ and diameter $D = 4.05\,mm$. Initially the pressure is kept constant at 40 bar and tests with different subcooling degrees are performed. The outlet pressure is 6.84 bar. An axisymmetric representation of the flow domain was used, using unstructured quadrilateral meshes of 24000 cells. The shape of the domain is shown in Fig. 1. Finer and coarser meshes with 60000 and 120000 cells were also used and results were found to be insensitive to grid resolutions.

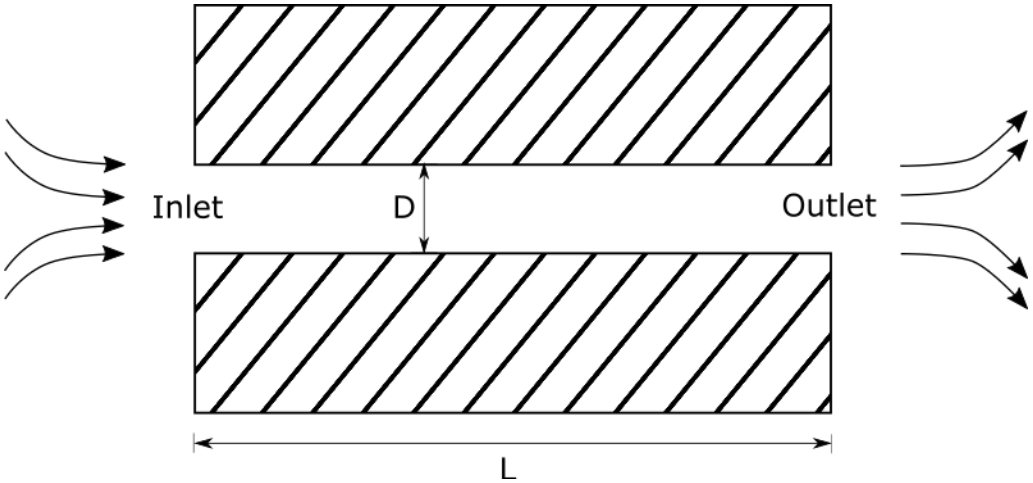

Fig 1: Schematic of the flow domain for the experiments of Jinliang et al. (1995)

Results for the calculated mass flow rates per area a.k.a. mass velocity are shown in Fig. 2. The mass flux is not derived from an explicit formulation: instead, it is given as the product of the mass-averaged velocity with the mixture density. The simulations are from the case of subcooling of 40℃ up to the superheated case. In the latter case, the mass flux becomes minimum in both experiments and simulations and the results are in good agreement with the data with a difference less than 5%. An instantaneous axisymmetric contour of the density and void fraction is shown in Fig. 3 for the case of zero subcooling. It is evident that the vapour generation begins at the nozzle inlet, right after the geometry changes. This vapour annulus surrounding the liquid core is also reported for cases of low $\boldsymbol{L/D}$ by Henry et al. (1970) and is also pronounced in cases of cavitation. The critical mass flow rates slightly increase by increasing the subcooling of the liquid in the storage conditions. Flow separation is observed downstream the inlet corner. In Fig. 4 the predicted mass flow rates are shown for a higher stagnation pressure of 160 bar. The pattern for the dependency on the subcooling is similar to the case of 40 bar inlet pressure. The observed trends for these two cases imply that for small $\boldsymbol{L/D}$ the subcooling degree of the inlet liquid is less influential on the critical mass flow rates. On the contrary, this is not the case for larger $\boldsymbol{L/D}$ ratios where Jinliang et al. (1995) showed that for nozzles with ratios equal or larger than 9.68 the critical mass flow rates of the pressurised water gradually change, following a steeper trend up to liquid with a subcooling degree equal to 40 ℃. Similar trends are also captured in the present study. Turbulent phenomena are expected to have impact on the mass flow rate at the exit but it is hard to quantify this dependency especially for small $\boldsymbol{L/D}$ where no dedicated studies exist for flahing. As shown in Fig. 4 the predictions for $\boldsymbol{k-\varepsilon}$ and SST $\boldsymbol{k-\omega}$ are in good agreement with the measurements. Fig. 5 shows the velocities at the inlet and oulet of the nozzle for some of the cases presented along the radial direction (R = D/2 is the radius of the pipe). The

characteristic parabolic velocity profile, common in single phase flows, is encountered here. At the centre of the pipe (r/R = 0) the velocity has its maximum value. Moving towards the nozzle walls, the axial velocity gradually decreases reaching its minimum at the wall boundary. Since the pressure drops along the axial direction, the downstream velocities are higher than the upstream with a ratio upstream-to-downstream velocity equal to approximatelely 0.63. The observations stand both for the subcooled and saturated flows, where velocity slightly changes. The peaks in the upstream velocities arise naturally due to the initiated cavitation caused by the flow separation shear layer at the low pressure area near the nozzle entrance.

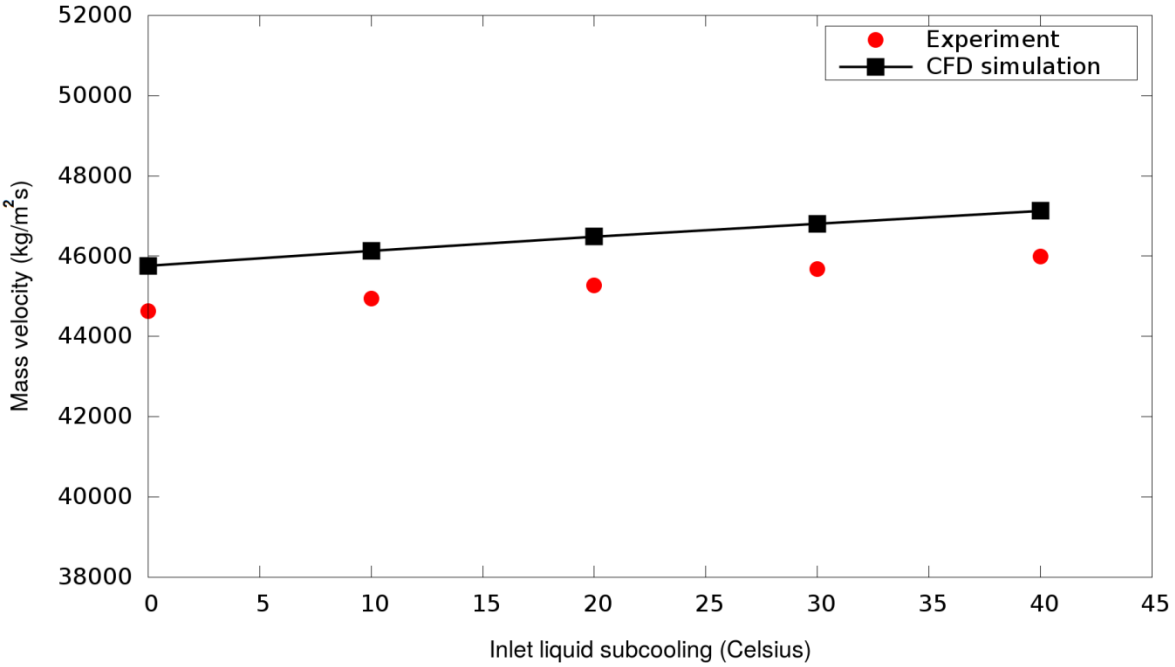

Fig. 2: The predicted mass flow rates per area for initial pressure equal to 40 bar compared to experimental data of Jinliang et al. (1995).

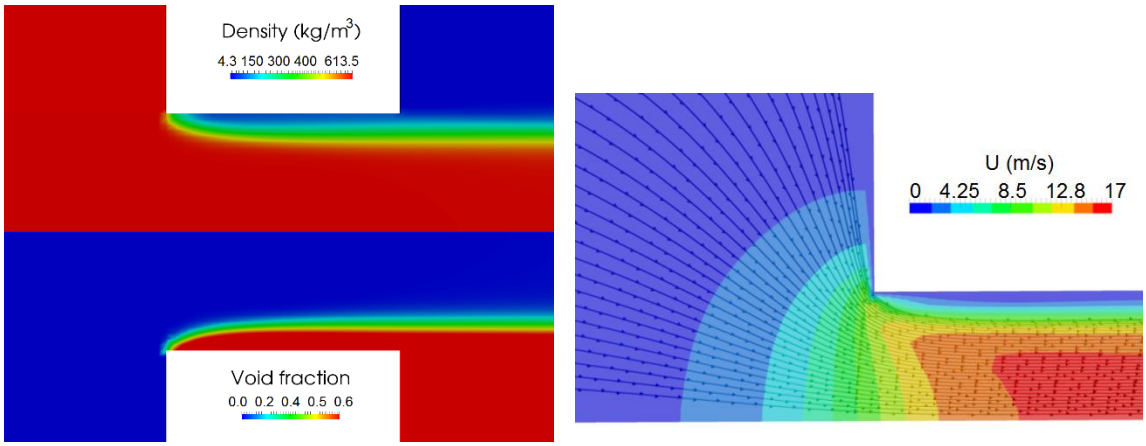

Fig. 3: The predicted instantaneous contours of the mixture density, void fraction and velocity profile for the case of 40 bar at the saturated conditions with same configuration as in the experiment of Jinliang et al. (1995).

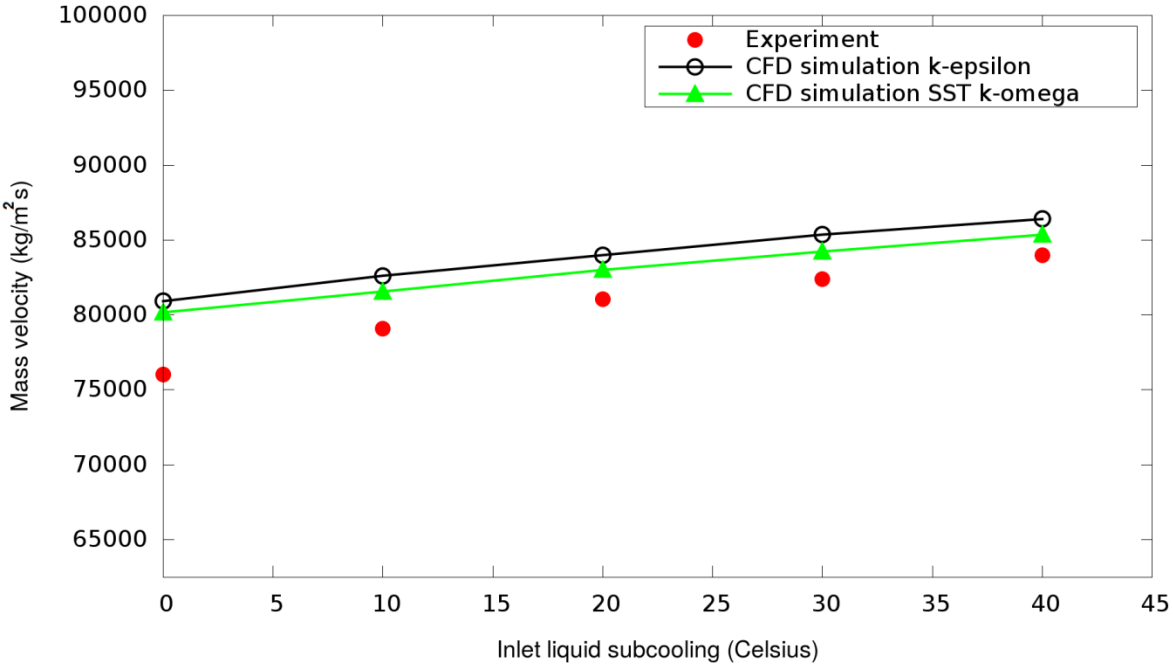

Fig. 4: The predicted mass flow rates per unit area for initial pressure equal to 160 bar compared to experimental data of Jinliang et al. (1995).

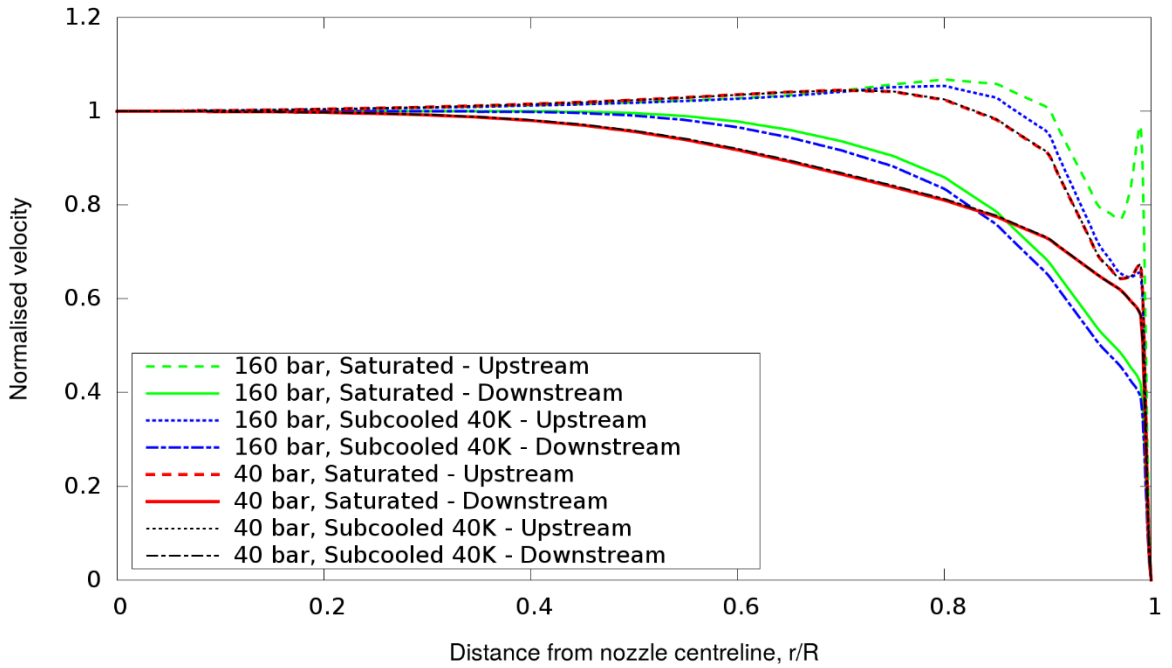

Fig. 5: The predicted velocities for different inlet pressures and temperatures upstream-downstream the nozzle.

The results presented so far are for flows with various subcooling degrees up to the saturated state. It is interesting to see how the presented method performs in only saturated inlet conditions. The results for the critical mass flow rate for different initial pressures keeping the same nozzle as before are demonstrated in Fig. 6. As soon as the single-phase liquid core starts to flow towards the exit, the pressure drops, following a trend that will be discussed in more detail next, resulting in a two-phase

jet at the end of the nozzle. The flashing inception is triggered when the jet pressure drops below the local saturation pressure. As mentioned in the experimental work used here for validation, the metastability of the flow starts at this point. The exact point where the flashing starts is non-trivial to determine, and there is no general model to predict it in the literature without limiting assumptions. The results are in good agreement, with a CFD-to-experiment difference generally less than 7%. The calculated void fraction is shown in Fig. 7. The void fraction is smaller in the centreline but increases closer to the wall as the result of the flow separation at the nozzle inlet. A qualitative perspective can be obtained from the void fraction, the pattern of which is more likely to change with increasing the ratio L/D as will be illustrated later. In all cases, the void fraction growth can be divided into three regions with respect to the distance from the centreline of the nozzle: from 0 to r/R equal to 0.15 it is almost constant, then increases on a log scale and from r/R between 0.8 and 1R grows fast to values that were usually around 0.45 in the nozzle inlet and close to the limit of unity at the nozzle end.

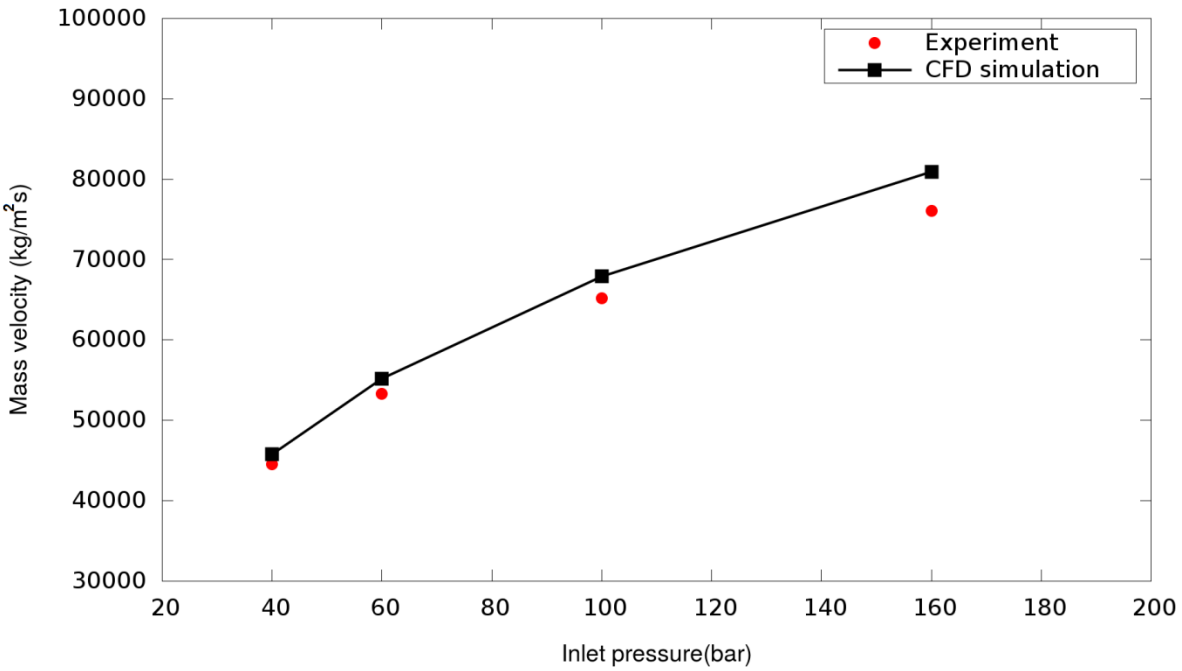

Fig. 6: The predicted mass flow rates per area for saturated stagnation conditions and different initial pressures up to 160 bar compared to experimental data of Jinliang et al. (1995).

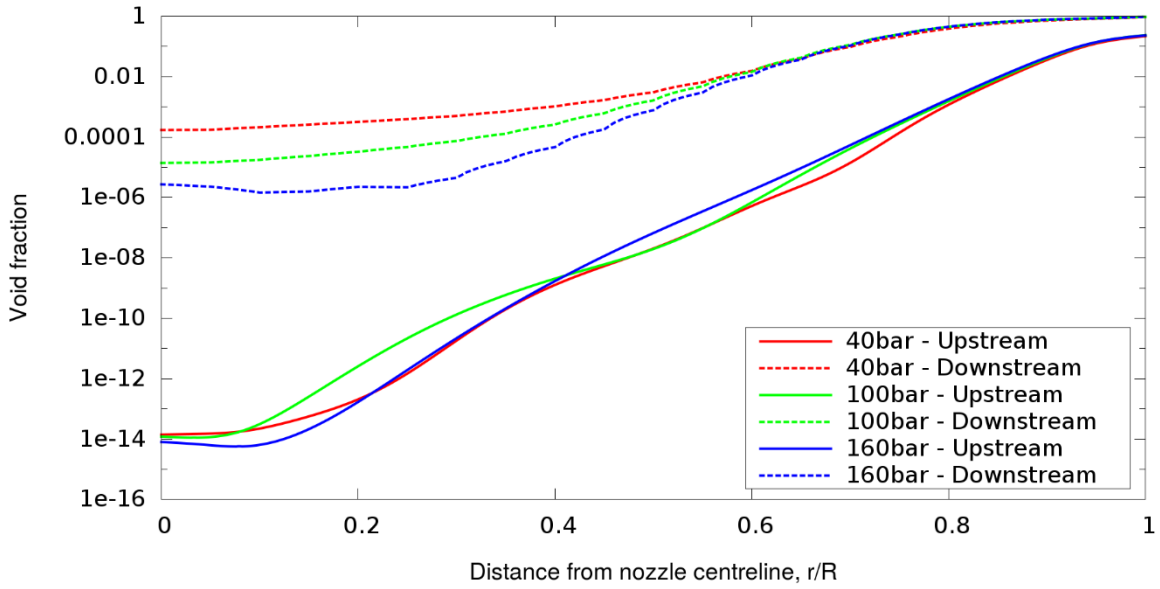

Fig. 7: The predicted void fraction in logarithmic scale for the upstream and downstream positions of the nozzle and various inlet pressures of initially saturated conditions.

3.2 *Turbulence and geometry impact on jet hydrodynamics*

The ratio of the nozzle length to diameter may also play a crucial role in the flashing affecting bubble nucleation and atomisation. There are no strict limits as to whether the flow will exihibit internal or external flashing mode. Following Witlox's (2002) review for flashing releases, one should expect the internal mode to be more likely to occur inside large nozzles although there is an uncertainty for short tubes. For nozzles with small L/D tested here, internal flashing occurs as well. The methodology developed in this study takes into account different parameters that could influence the correct mass flow rate calculation such as the compressibility and turbulence effects.

Pressure gradients are always present during liquid flow through the pipe, which cannot be a-priori estimated. A small pressure gradient may play a significant role in the momentum transport. Radial pressure gradients in turbulent pipe flows have been previously reported and seen that are an increasing function of Reynolds number. According to Iciek (1982) for long sharp-edged orifices of $L/D > 5$ turbulence is expected to be generated before the nozzle exit. On the other hand, for smaller L/D ratios, the inertial forces are likely to dominate viscous forces. A transition from laminar to turbulent regime is possible to occur in these cases, exhibiting a larger effect of L/D on the flow regime.

Since the validated numerical investigations for nozzles with large L/D ratios employing the HRM is scarce, a second series of simulations is included in the present study. Park et al. (1997) performed simulations for various nozzle lengths for flashing water released to nearly atmospheric conditions. Different inlet liquid pressures and subcooled degrees were investigated to extrapolate a correlation for the critical mass flow rates using various L/D. Here the case of $L/D = 29.4$ is studied. The fluid flows through a pipe with diameter $D = 3.4mm$ and length $L = 100mm$ using a similar shape apparatus as in the previous experiment. In Fig. 8 the calculated mass flux is ploted against the initial liquid temperature for constant inlet pressure equal to 10 bar. Three meshes of 30000, 60000 and 150000 were tested using the same boundary conditions as before except for the fixed pressure and temperature. The computational mesh was refined close to the nozzle walls so that the liquid/gas interphase is resolved and the mesh resolution is considered significantly smaller than the interfacial curvature radius. Here the results obtained from the coarsest mesh are demonstrated. The saturated temperature is 180℃. This corresponds to the lowest mass flow rate shown in the graph. The mass flow rate follows the same trend as in the case of the sharp-edged orifice demonstrated before, only in

this case the evaporation rate has more impact on the critical mass flow rate, hence a steeper mass flow rate curve.

The pressure distribution within the pipe has also been studied. In flashing cases, the pressure drop is expected to be high and can be close to 50% of the initial storage pressure (Jinliang et al. 1995). In Fig. 9 the predicted pressure across the pipe is shown for two different initial temperatures. The first case is for the saturated state and the second one for a subcooling degree equal to 11 ℃. The stagnation pressure for both cases is 15 bar. In both cases, the same pattern is observed, which is the rapid pressure drop in the sharp inlet corner where the flow separates, and phase change starts. It is worth mentioning that the pressure at that point is, in both the experimental and numerical study, above the local saturation which implies that flashing is triggered downstream of the corner. Another interesting finding providing newer insights is that the pressure drop is generally higher in the subcooled case, meaning that the pressure along the pipe is more likely to be higher compared to the saturated inlet for the same initial pressure. The pressure difference in the case of subcooling degree of 11 ℃ is approximately one bar within the pipe up to the position which corresponds to the 85% of the pipe length, L.

The relationship of pressure distribution with respect to the stagnation pressure of the liquid is investigated next. In Fig. 10 the cases of inlet pressures of 15 bar and 10.15 bar are compared for the case of initially subcooled water at 169 ℃. Surprisingly, the pressure drop downstream the inlet corner is the same in both cases, and the pressure profile is almost the same after the position of 5% of the pipe length. This can be interpreted that the pressure distribution within the nozzle is more sensitive in the subcooling degree than the initial pressure at the inlet, at least for nozzles with the relatively large length-to-diameter ratio. Increasing the L/D ratio, the mixture has more time to fully develop inside the nozzle. The effects of turbulent mixing become more importnant and the change in flow regime from pure liquid to bubbly is enhanced. Testing the water jet at 15 bar of Park et al. keeping the same diameter but for L/D equal to one, an indication for the L/D impact on the regime can be obtained. In Fig. 11 the void fraction for both cases has a similar trend with a larger minimum value and almost double for L/D = 29.4. Results of Fig. 7 demonstrate a smaller void fraction at the centreline for larger pressures with the one at 40 bar to be 10^4 times smaller. Nevertheless the diameter in Fig. 11 was 3.4 mm and not the same as in the case illustrated in Fig. 7 (D = 4 mm).

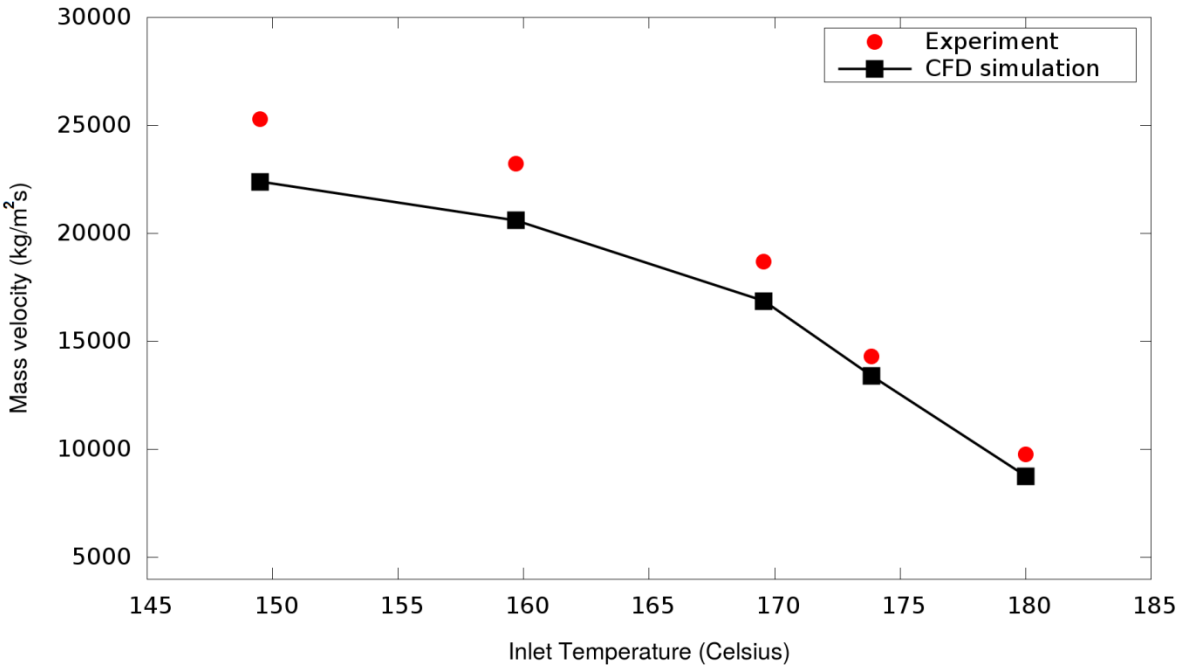

Fig. 8: The predicted mass flow rates per area for different initial temperatures compared to experimental data of Park et al. (1997).

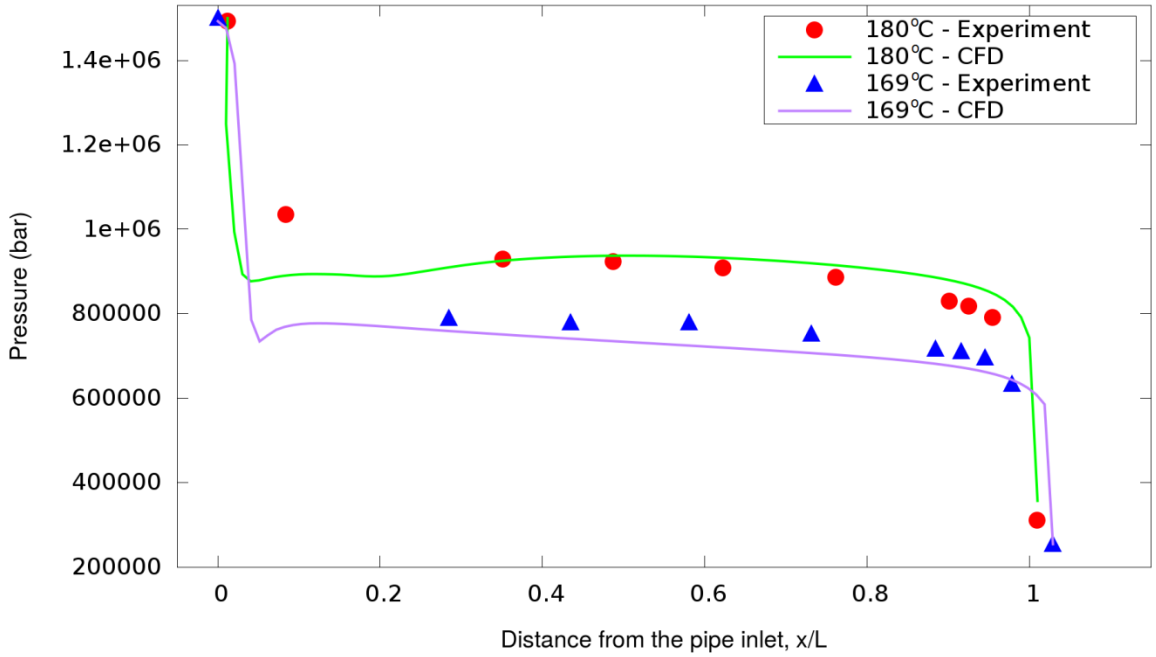

Fig. 9: The predicted pressure distribution along the pipe for different inlet temperatures for L/D=29.4.

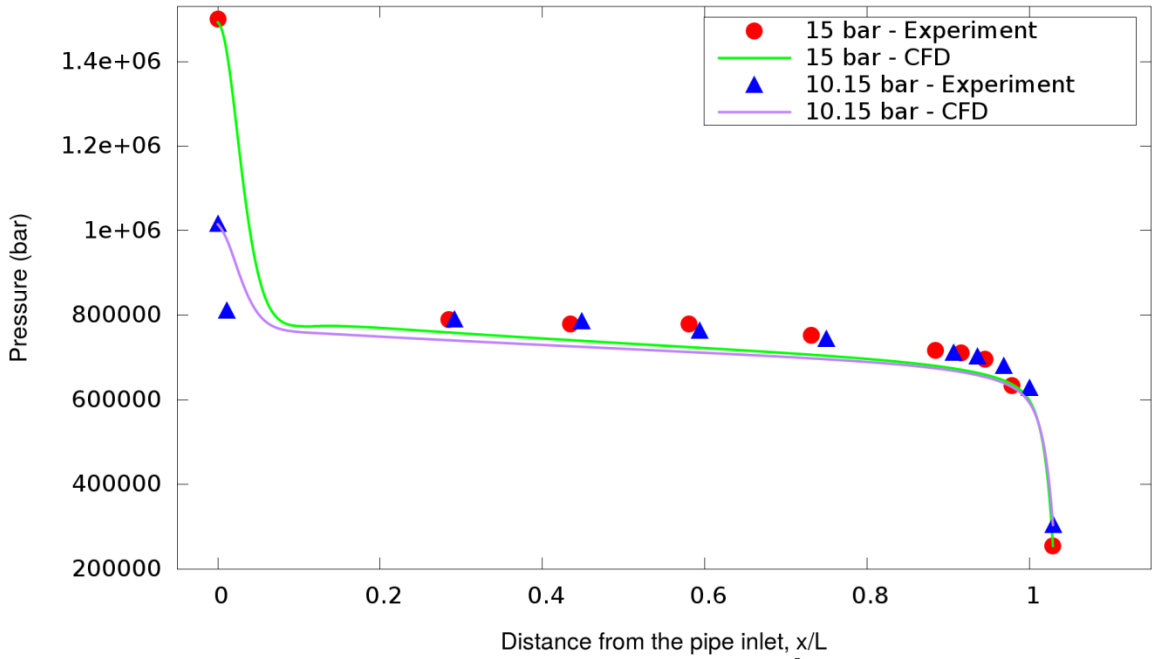

Fig. 10: **The predicted p**ressure distribution inside the pipe for 169.4 ^{o}C and different initial pressures.

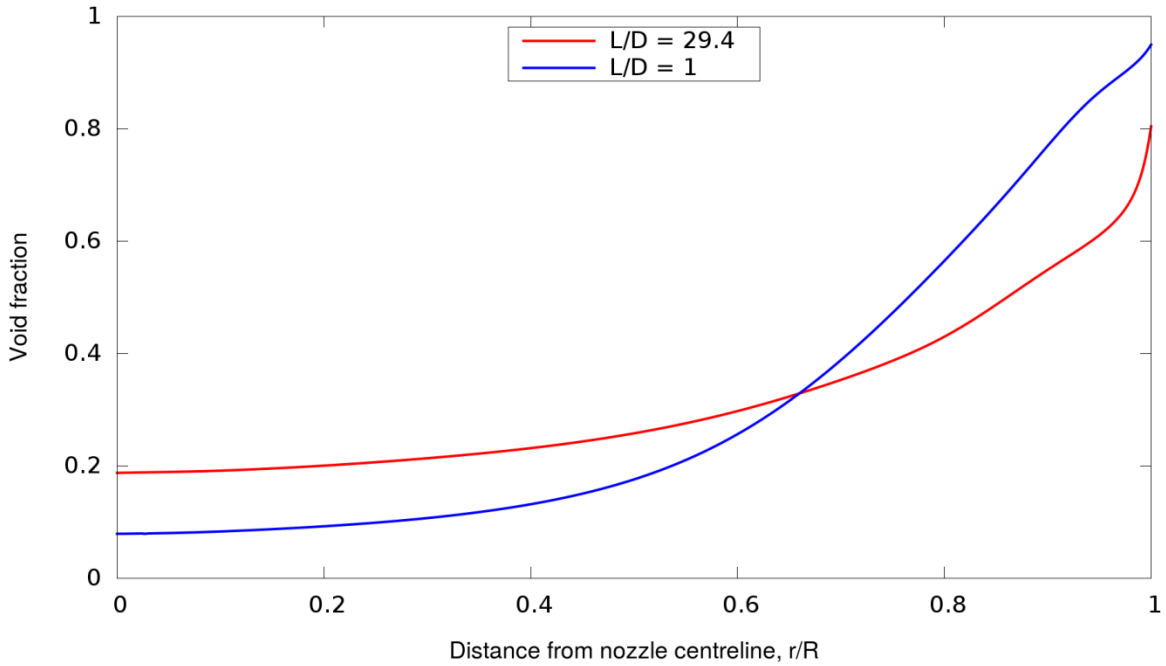

Fig. 11: The predicted void fraction for inlet pressure equal to 15 bar and different L/D for water flow.

3.3 *Flashing in cryogenic liquids*

The developed model has been applied to predict the flashing of cryogenic liquids flowing through short pipes. Such applications of the model is another novel aspect of the current work. The outlet pressure (end of nozzle) is set to 1 bar. Liquid Nitrogen and R134a (1,1,1,2-tetrafluoroethane), which were initially in saturated conditions at 15 bar in the storage vessel, are considered. The computational domain is similar to the one in Fig. 1. Two dimensional simulations were conducted for qualitative comparisons. Different mesh refinement levels were used for these simulations with the dimensionless wall distance, being around 300, 200, 100, and 10. The diameter (D = 2 mm) of the nozzle is kept constant like in all the previous cases and the length-to-diameter ratio L/D is equal to 2. The axial

velocity at the upstream and downstream positions presented in Fig. 12 is divided by the maximum one for simplicity and plotted with respect to the whole nozzle diameter (r/R = 0 denotes the centre of the circular profile). The axial velocity is smooth close to the position of the maximum velocity at r/R = 0 but gradually changes when moving closer to the walls. The change in the velocity gradient occurs at almost the same distance for all the liquids at the downstream position. In the upstream case, the velocity profile becomes non-monotonic a bit further away from the wall and the velocity profile follows the patterns shown in Fig. 5. The same patterns appear in Winkhofer et al. (2001) where the cavitation gas exists in the shear layer enhancing the velocity peak. It is interesting that the patterns in velocity within the nozzle are similar for cryogenic and non-cryogenic fluid. The void fraction is expected to have its maximum in the recirculation zone close to the wall and becomes minimum at the centreline. Fig. 13 shows this trend for the void fraction. The centreline void fraction can vary in the position r/R = 0 and the difference in the volume occupied by the vapour is more extensive for the three liquids at the nozzle exit with a correspondingly different regime. One of the advantages of the presented methodology is that it can offer an estimation for the thickness of the vapour layer formed in the walls.

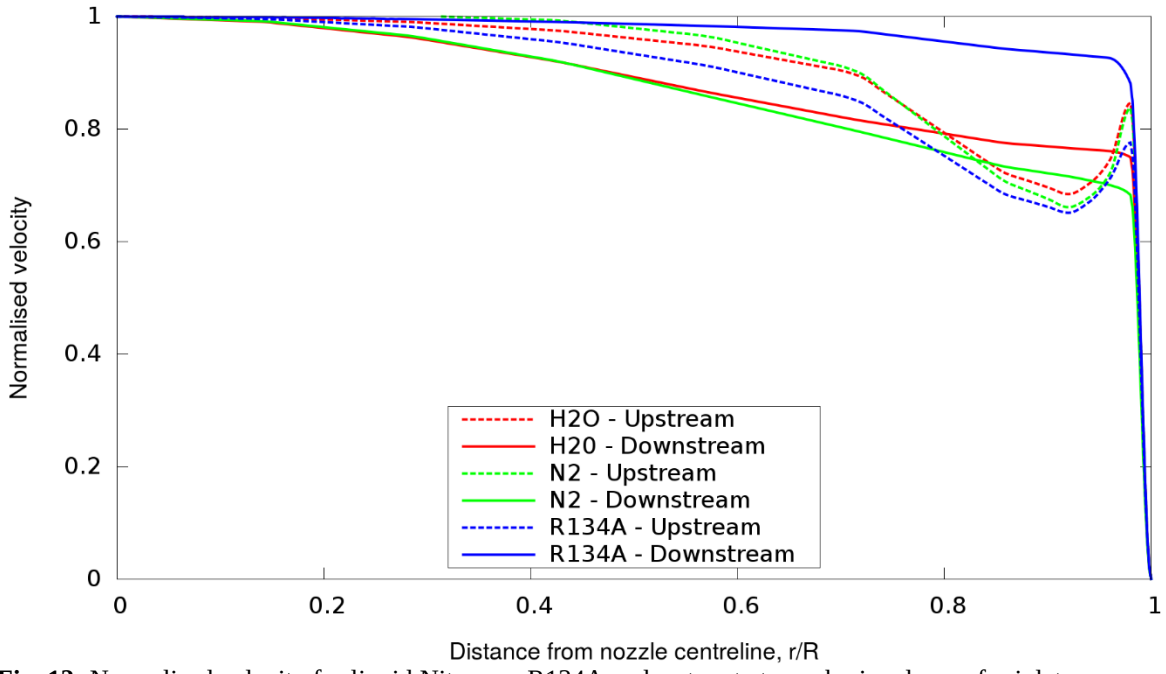

Fig. 12: Normalised velocity for liquid Nitrogen, R134A and water at atmospheric releases for inlet pressure 15 bar and L/D = 2.

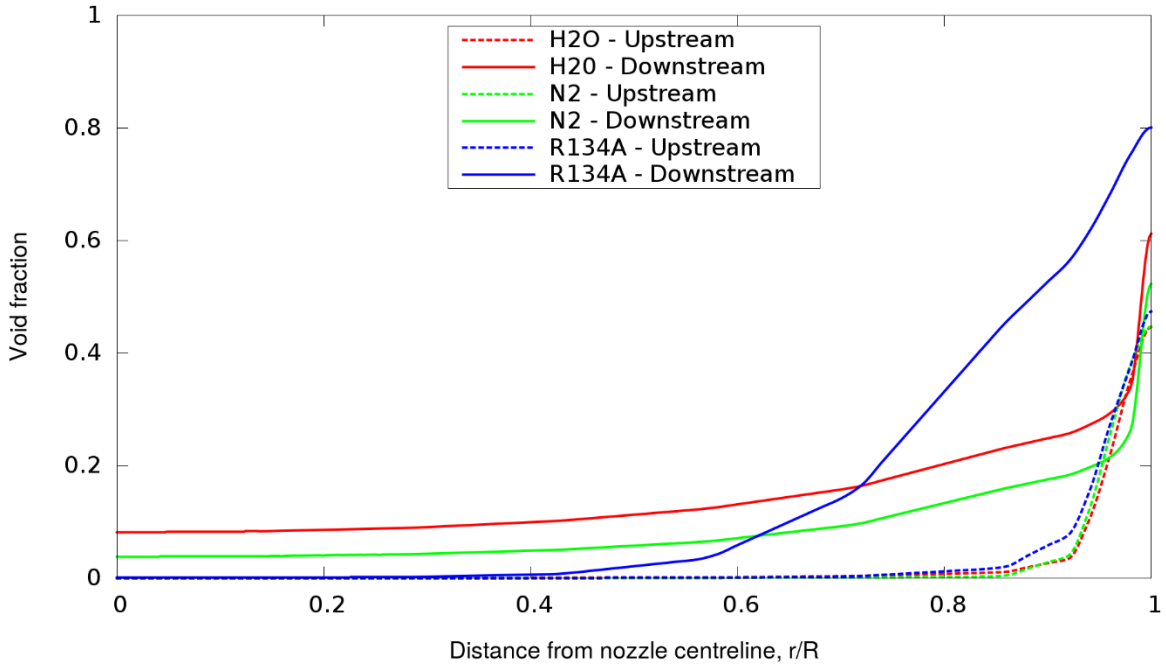

Fig. 13: Void fraction versus the distance from the centreline for the three liquids.

Conclusions

FlashFOAM, a new compressible solver has been developed within the frame of open source CFD code OpenFOAM to compute phase change within various nozzle and orifice geometries experiencing rapid pressure drops. FlashFOAM is capable of simulating flashing and the impact of bubble nucleation on the flow, and is validated using experiments with both subcooled and saturated initial conditions. The mass flow rates at the validated cases are close to those observed in the experiments. The predictions confirmed experimental findings that indicate a two-phase jet at the nozzle exit which continues evaporating downstream. The void fraction trends show an annular flow regime. In the presented method the liquid phase is tracked, and uses a novel pressure update. This pressure correction which is in the heart of the PIMPLE algorithm includes the effects of flash-boiling, ambient air entrainment and interfacial forces in a new numerical approach. Turbulence modelling is found to play a major role for accurate predictions of the mass flow rates and the $k-\varepsilon$ model appears to be adequate for the geometries presented. The model has been tested within the RANS framework but it can be implemented in the Large Eddy Simulations (LES) context as well to give more accurate predictions of primary atomisation. Models for the spray dynamics can be easily implemented and together with the VOF method the methodology presented can be used to derive a unified methology to simulate the whole process of liquid atomisation starting from inside the nozzle until the jet shatters to small droplets.

Further numerical simulations have also been conducted for the flashing of cryogenic liquids. Patterns of flow characteristics indicate that the heat and mass transfer is important in cryogenic liquids that flash through pipes. The thermal non-equilibrium model employs a semi-empirical correlation validated for water data. This correlation has also been tested for cases involving other liquids (liquid nitrogen, R134A) and found adequate for predicting the void fraction. Additional tests for calibrating the HRM parameters for these liquids and different depressurisation regimes in moderate superheat degrees could be conducted in the future. Coupling HRM with bubble growth models could provide a more detailed insight of the physics inside the pipe. This could be also possible with a two-fluid approach and with a careful selection of the additional assumptions that are

introduced to the problem. The current work needs to be extended to include the effects of the sub-grid scale turbulence for resolving more accurately the bubble dispersion patterns in the flow.

Acknowledgements

The authors wish to thank the Marie Curie Action of the 7th Framework Programme of the European Union. The current work is part of the SafeLNG project (Project ID: 606754) regarding the Numerical characterization and simulation of the complex physics underpinning the Safe Handling of Liquefied Natural Gas (2014-2017).

References

Bianchi, G. M., Forte, C., Negro, S. and Pelloni, P., 2008.A 1d Model for the Prediction of Flash Atomization in GDI Multi-Hole Injectors: Preliminary Results. SAE Technical Paper Series, no. 2008-01-2516..

Bilicki, Z, and Kestin, J., 1990. Physical aspects of the relaxation model in two¬phase flow. Proceedings of the Royal Society of London. Series A, Mathematical and Physical Sciences, 379-397.

Brackbill, J.U., Kothe, D.B., Zemach, C., 1992. A continuum method for modelling surface tension. J. Comput. Phys. 100, 335-354.

Downar-Zapolski, P., Bilicki, Z., Bolle, L. and Franco, J., 1996. The Non-Equilibrium Relaxation Model for one-dimensional Flashing Liquid flow. International Journal of Multiphase Flow 22,3, 473-483.

Einstein, A., 1920.Uber Schallschwingungen in teilweise dissoziierten Gasen. Sitzung Berl. Akad. Physik Chemie, 380-385

Fauske, H.K., 1962. Contribution to the Theory of Two-Phase. One Component Critical Flow. Argonne Natl. Lab. Tech. Report ANL-6633.

Fujimoto, H., Nishikori, T., Hojyo, Y., Tsukamoto, T., and Senda, J., 1994. Modelling of Atomisation and Vaporisation Process in Flash Boiling Spray. The International Conference on Liquid Atomisation and Spray Systems, Paper VI-13, Rouen.

Henry, RE., 1970.The two-phase critical discharge of initially saturated or subcooled liquid. Nuclear Science Engineering41 336–342.

Iciek, J., 1982. The hydrodynamics of a free, liquid jet and their influence on direct contact heat transfer - I and II. Int. J. Multiphase Flow 8 3, 239–260.

Ishimoto, J., Ohira, K., Okabayashi, K. and Chitose, K., 2009. Integrated Numerical Prediction of Atomization Process of Liquid Hydrogen Jet. J. Cryo. Soc. Jpn. 44, 7.

Issa, R.I., 1986. Solution of the implicitly discretised fluid flow equations by operator-splitting. J. Comput. Phys. 62, 40–65.

Jasak, H., 1996. Error Analysis and Estimation for the Finite Volume Method with Applications to Fluid Flows, Ph.D Thesis, Imperial College of Science, Technology and Medicine, London.

Jiang, X., Siamas, G.A., Jagus, K., Karayiannis, T.G., 2010. Physical modelling and advanced simulations of gas liquid two-phase jet flows in atomization and sprays. Progress in Energy and Combustion Science 36 131-167.

Jinliang, Xu, Tingkuan, Chen, T., Yang, L., 1995. Two-Phase Critical Discharge of Initially Saturated or Subcooled Water Flowing in Sharp-Edged Tubes at High Pressure. J. of Thermal Science 4, 3, 193-199.

Lee, .J, Madabhushi, R., Fotache, C., Gopalakrishnan, S., Schmidt, D., 2009. Flashing flow of superheated jet fuel. Proceedings of the Combustion Institute 32 3215–3222.

Yixiang, Liao, Lucas, Dirk, 2015. 3D CFD simulation of flashing flows in a converging-diverging nozzle, Nuclear Engineering and Design 292 149–163.

Maksic, S., Mewes, D., 2002. CFD-calculation of the flashing flow in pipes and nozzles. Proc. of ASME FEDSM'02, Montreal, Quebec, Canada, 14–18.

Moody, F.J., 1965. Maximum Flow Rate of a Single Component, Two-Phase Mixture. J. Hear Transfer 87 134- 141.
Menter, F.R., 1993. Zonal Two Equation k-ω Turbulence Models for Aerodynamic Flows. AIAA Paper 93-2906.
Oza, R.D., and Sinnamon, J.F., 1983. An experimental and analytical study of flash boiling fuel injection. *SAE Paper* 830590.
Park, B.S. and Lee, S.Y., 1994. An Experimental Investigation of the Flash Atomisation Mechanism. Atomisation and Sprays, 4 159-179.
Patankar, S. V., 1980. Numerical Heat Transfer and Fluid Flow. Hemisphere Publishing Corporation, New York.
Park, C-K, Park, J-W, Chung, M-K, and Chung, M-H., 1997. An empirical correlation for the Critical Flow Rates of Subcooled Water Through Short Pipes with Small Diameters. Journal of the Korean Nuclear Society, 29 1, 35-44, 1997.
Poinsot, T.J., and Lele, S.K., 1992. Boundary Conditions for Direct Simulations of Compressible Viscous Reacting Flows. Journal of Computational Physics, 101, 104-129.
Prosperetti, A., Tryggvason, G., 2006. Computational Methods for Multiphase Flow, Cambridge University Press.
Reinke, P., Yadigaroglu, G., 2001. Explosive vaporisation of superheated liquids by boiling fronts. Int. J. Multiphase Flow, 27, 1487-1516.
Rusche, H., 2002. Computational fluid dynamics of dispersed two-phase flows at high phase fractions. PhD thesis, Imperial College London.
Salvador, F. J, Jaramilloa, D., Romero, J.V., Roselló, M.D., 2017. Using a homogeneous equilibrium model for the study of the inner nozzle flow and cavitation pattern in convergent–divergent nozzles of diesel injectors. Journal of Computational and Applied Mathematics 309, 630–641.
Schmidt, D.P, Gopalakrishnan, S., Jasak, H., 2010. Multi-dimensional simulation of thermal non-equilibrium channel flow. International Journal of Multiphase Flow 36, 284–292.
Schroder, Jens Jurgen, and Nha, Vuxuan, 1987. Homogeneous Non-Equilibrium Two-Phase Critical Flow Model. Chem. Eng. Technol. 10, 420-426.
Sher, Eran, Tali, Bar-Kohany, Rashkovan, Alexander, 2008. Flash –boiling atomization. Progress in Energy and Combustion Science 34, 417-439.
Srinivasan, V., Salazar A., Sait, K., 2010. Modeling the disintegration of cavitating turbulent liquid jets using a novel VOF–CIMD approach. Chemical Engineering Science 65, 2782–2796.
Wareing, Christofer J., Fairweather, Michael, Falle, Samuel, A.E.G., Woolley, Robert, M., 2014. Validation of a model of gas and dense phase CO2 jet releases for carbon capture and storage application. International Journal of Greenhouse Gas Control 20, 254–271.
Weller, Henry, Tabor, G., Hrvoje, Jasak, Fureby, C., 1998. A tensorial approach to computational continuum mechanics using object-oriented techniques. Comput. Phys. 12, 620–631.
Wen, Jennifer, Heidari, Ali, Xu, Baopeng and Jie, Hongen, 2013. Dispersion of carbon dioxide from vertical vent and horizontal releases-A numerical study. Proc IMech Part E: J Process Mechanical Engineering 227 2, 125-139.
Wen, Jennifer, X, Le Fur, Pierre, Jie, Hongen, and Vendra, C. Madhav, Rao, Further development and validation of CO_2FOAM for the atmospheric dispersion of accidental releases from carbon dioxide pipelines, International Journal of Greenhouse Gas Control, Volume 52, September 2016, Pages 293-304.
Winklhofer, E., Kull, E., Kelz, E., and Morozov, A., 2001. Comprehensive hydraulic and flowfield documentation in model throttle experiments under cavitation conditions. ILASS Europe.
Witlox, H., Bowen, P.J,. 2002. Flashing liquid jets and two-phase dispersion A review. Contract research report 403/2002, HSE.
Zaloudek, F.R., 1964. Steam-water critical flow from high pressure systems. Interim reportGeneral Electric Co., Richland, WA, United States. Hanford Atomic Products Operation, Washington, DC, United States HW-80535-RD.